Structural insights into the N-terminal GIY–YIG endonuclease activity of *Arabidopsis* glutaredoxin AtGRXS16 in chloroplasts

Xi Liu[a], Shian Liu[b,1], Yingang Feng[c,2], Jian-Zhong Liu[d], Yuling Chen[a], Khanh Pham[b], Haiteng Deng[a], Kendal D. Hirschi[b], Xinquan Wang[a,2], and Ninghui Cheng[b,2]

[a]Ministry of Education Key Laboratory of Protein Science, Center for Structural Biology, School of Life Sciences, Tsinghua University, Beijing 100084, China; [b]USDA/ARS Children Nutrition Research Center, Department of Pediatrics, Baylor College of Medicine, Houston, TX 77030; [c]Shandong Provincial Key Laboratory of Energy Genetics, Qingdao Institute of Bioenergy and Bioprocess Technology, Chinese Academy of Sciences, Qingdao, Shandong 266101, China; and [d]College of Chemistry and Life Science, Zhejiang Normal University, Jinhua, Zhejiang 321004, China

Edited by Bob B. Buchanan, University of California, Berkeley, CA, and approved April 23, 2013 (received for review April 12, 2013)

Glutaredoxins (Grxs) have been identified across taxa as important mediators in various physiological functions. A chloroplastic monothiol glutaredoxin, AtGRXS16 from *Arabidopsis thaliana*, comprises two distinct functional domains, an N-terminal domain (NTD) with GlyIleTyr-TyrIleGly (GIY-YIG) endonuclease motif and a C-terminal Grx module, to coordinate redox regulation and DNA cleavage in chloroplasts. Structural determination of AtGRXS16-NTD showed that it possesses a GIY–YIG endonuclease fold, but the critical residues for the nuclease activity are different from typical GIY–YIG endonucleases. AtGRXS16-NTD was able to cleave λDNA and chloroplast genomic DNA, and the nuclease activity was significantly reduced in AtGRXS16. Functional analysis indicated that AtGRXS16-NTD could inhibit the ability of AtGRXS16 to suppress the sensitivity of yeast *grx5* cells to oxidative stress; however, the C-terminal Grx domain itself and AtGRXS16 with a Cys123Ser mutation were active in these cells and able to functionally complement a Grx5 deficiency in yeast. Furthermore, the two functional domains were shown to be negatively regulated through the formation of an intramolecular disulfide bond. These findings unravel a manner of regulation for Grxs and provide insights into the mechanistic link between redox regulation and DNA metabolism in chloroplasts.

reactive oxygen species | nuclear magnetic resonance

Reactive oxygen species (ROS) can be formed as by-products in all oxygenic organisms during aerobic metabolism (1). In higher plants, chloroplasts/plastids and mitochondria are two major organelles that contribute to the production of ROS during photosynthesis and carbon metabolism (2). Because of their cytotoxic and reactive nature, ROS can cause wide-ranging damage to macromolecules, such as proteins, lipids, and DNA (3). Photoprotection of photosynthetic apparatus and genomic DNA from oxidative-induced damage are critical for chloroplast function and plant survival under extreme conditions (4). Cells have thus orchestrated an elaborate antioxidant network to overcome such oxidative damage and control signaling events (5).

Glutaredoxins (Grxs) are disulfide oxidoreductases (thioltransferase) and play an important role in scavenging cellular ROS and regulating redox homeostasis (6). Grxs can be categorized into two major classes, dithiol Grxs that contain two cysteine residues and monothiol Grxs that contain a single cysteine residue in their putative motifs (6). Among monothiol Grxs, CGFS-type Grxs which contain a conserved Cys-Gly-Phe-Ser (CGFS) motif were initially identified in yeast, then subsequently identified in numerous other organisms (7). Recent advances in the biochemical analysis of CGFS-type Grxs suggest conserved structural features and the interchangeability of their functions (7). CGFS-type Grxs from plants and metazoan are able to perform the functions of *Saccharomyces cerevisiae* Grx5 (ScGrx5) in the biogenesis of Fe-S clusters in yeast mitochondria (8). However, *Plasmodium falciparum* glutaredoxin-like protein 1 (PfGLP1) does not bind a Fe-S cluster (9) and in *Pteris vittata* Grx5 (PvGrx5), the Cys^{67} residue at the N-terminal region, not the Cys^{108} at the "CGFS" motif, is required for Grx activity and arsenic resistance (10). These results suggest diverse regulation among various CGFS-type Grxs, but the underlying mechanisms remain to be fully investigated.

The GlyIleTyr-TyrIleGly (GIY-YIG) motif was initially identified in a group of homing endonucleases (11). In the short motif GIY, Gly can be Val or Leu and Ile can be Val; In the short motif YIG, Tyr can be Phe or Lys and Ile can be Val. The space between the two short motifs can vary (12). The GIY–YIG endonuclease superfamily has been implicated in DNA rearrangements and recombination, nonspecific DNA degradation, DNA repair, and maintenance of genome stability (12). Putative GIY–YIG endonucleases have been identified in chloroplasts (13). Initial studies suggest that this type of GIY–YIG endonucleases may play a critical role in repairing oxidative stress-induced DNA double-strand breaks (DSB) in plants (14). A recent study implicates that activation of phage T4 intron endonuclease, I-TevI, is redox-dependent (15), suggesting that there may be a link between endonuclease activity and redox homeostasis.

AtGRXS16, initially termed CXIP2 (16), was originally identified in a yeast screen looking for activation of transport activity. Like AtGRXS14 and AtGRXS15 (17, 18), AtGRXS16 consists of a conserved C-terminal Grx domain (CTD). However, AtGRXS16 contains a putative N-terminal domain (NTD) with GIY-YIG endonuclease motif that appears to be distinct from any known Grx. Here, we examined the subcellular localization of AtGRXS16. Using site-directed mutagenesis approaches and yeast functional assays, we characterized the function and regulation of AtGRXS16. We further determined the structure of AtGRXS16-NTD and defined its biochemical properties. Our results provide insights into the mechanistic link between redox regulation and DNA metabolism in chloroplasts.

Results

Structure of AtGRXS16-NTD Adopts a GIY–YIG Endonuclease Fold with Unique Catalytic Residues. AtGRXS16 is one of four CGFS-type monothiol Grxs in *Arabidopsis* and targets to chloroplast (Fig. S1). AtGRXS16 contains a long N-terminal extension with about 100 amino acids (Fig. S2). This N-terminal domain appears to be

Author contributions: Y.F., X.W., and N.C. designed research; X.L., S.L., Y.F., J.-Z.L., Y.C., K.P., H.D., and N.C. performed research; Y.F., X.W., and N.C. analyzed data; and Y.F., K.D.H., X.W., and N.C. wrote the paper.

The authors declare no conflict of interest.

This article is a PNAS Direct Submission.

Data deposition: The atomic coordinates have been deposited in the Protein Data Bank, www.pdb.org (PDB ID code 2LWF) and the NMR chemical shifts have been deposited in the BioMagResBank, www.bmrb.wisc.edu (accession no. 18624).

[1]Present address: Department of Biology, Texas A&M University, College Station, TX 77843.

[2]To whom correspondence may be addressed. E-mail: ncheng@bcm.edu, xinquanwang@mail.tsinghua.edu.cn, or fengyg@qibebt.ac.cn.

This article contains supporting information online at www.pnas.org/lookup/suppl/doi:10.1073/pnas.1306899110/-/DCSupplemental.

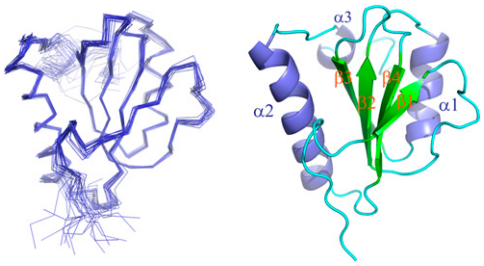

Fig. 1. Structure of AtGRXS16-NTD. (*Left*) The backbone ensemble of 20 structures of AtGRXS16-NTD. (*Right*) The ribbon representation.

plant-specific and conserved among the members of different plant species (Fig. S2). Most interestingly, this NTD comprises a putative GIY–YIG motif that belongs to the GIY–YIG nuclease superfamily (11, 12).

The determined solution structure of AtGRXS16-NTD shows that it adopts an expected mixed α/β topology (β1–β2–β3–α1–β4–α2–α3), built around a central anti-parallel β sheet (β2, β3, and β4) (Table S1 and Fig. 1). In general, AtGRXS16-NTD has a very similar architecture to bacterial GIY-YIG endonuclease UvrC and I-TevI (Fig. S3*A*), which are also the closest neighbors revealed by searching against the Dali database. The conserved antiparallel β sheet of AtGRXS16-NTD is further expanded with an extra N-terminal hairpin including the short β1, which is absent in UvrC and I-TevI (Fig. S3*A*). Compared with other GIY–YIG endonucleases with known 3D structures [Bacteriophage T4 endonuclease II (T4 EndoII), *Escherichia coli* 29K restriction endonuclease (R.Eco29KI), and *Helicobacter pylori* 188 restriction endonuclease (Hpy188I)], the GIY–YIG fold of AtGRXS16-NTD is more compact with less secondary structure and loop "decorations" (Fig. S3*B*).

AtGRXS16-NTD is different from other previously studied GIY–YIG endonucleases in the signature sequence motifs, catalytic and metal-binding residues, and DNA-recognizing residues in the GIY–YIG core region. Previously identified signature sequence motifs include the "GIY" and the "YIG" in the N-terminal part, an arginine residue in the center, and a glutamate residue in the C-terminal region (Fig. 2*A*). The conserved tyrosine, arginine, and glutamate are critical for the catalytic activity (19). In AtGRXS16-NTD, the GIY and the YIG motifs, located in the β2 and the β3 strands, are replaced with the "GVY" and the "FVG," respectively (Fig. 2 *A* and *B*). The arginine in the α1 helix and the glutamate in the α2 helix are substituted with serine and tryptophan, respectively (Fig. 2 *A* and *B*). In R.Eco29KI, the nuclease active site consists of Tyr49, Tyr76, Arg104, His108, Glu142, and Asn154 (19). AtGRXS16-NTD has a similar catalytic geometry as R.Eco29KI (Fig. 2*C*), and the corresponding residues Tyr90, Phe101, Ser111, His115, Trp143, and Asn161 are highly conserved among different plant species (Fig. S2). However, three of these residues (Phe101, Ser111, Trp143) are different from the conserved residues in other GIY–YIG endonucleases, including the replacement of the conserved glutamate that is critical for metal binding (Glu142 in R. Eco29KI) with Trp143 in AtGRXS16-NTD (Fig. 2*A*). The DNA-recognizing residues in the GIY–YIG core region of R. Eco29KI (Lys79 and Arg104) and Hpy188I (His76 and Arg84) are also not conserved in AtGRXS16-NTD (Ile104 and Ser111). Instead, AtGRXS16-NTD has positively charged regions formed by Arg106, Lys136, Lys144, and Lys170, which surround the putative nuclease active site and are conserved in all plant GRXS16 members (Fig. S2). These differences raise the question whether AtGRXS16-NTD has altered nuclease activities.

AtGRXS16 NTD Comprises Endonuclease Activity. The fact that AtGRXS16-NTD has a putative GIY–YIG endonuclease fold led us to further investigate its endonuclease activity in vitro. Because there is no knowledge about the native substrate of AtGRXS16-NTD, we used linearized λDNA as a substrate in the nuclease assay experiments. We found that AtGRXS16-NTD had an intrinsic Mg^{2+}-dependent endonuclease activity in vitro (Fig. 3*A*), which was able to cleave the linearized λDNA into smear bands in

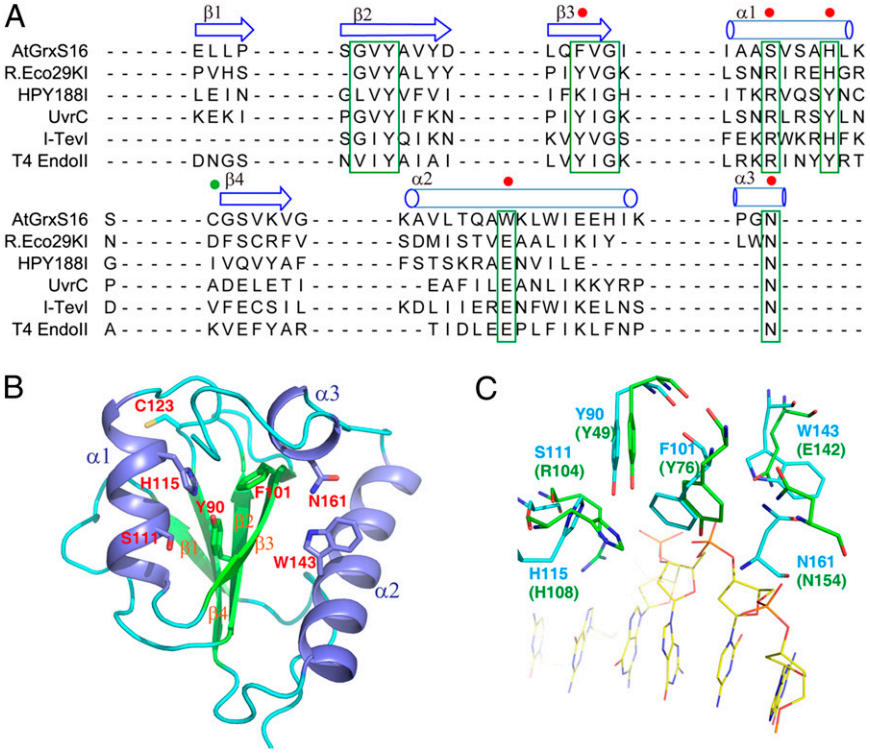

Fig. 2. Comparison of GIY–YIG signature sequence motifs and catalytically important residues between AtGRXS16-NTD and other GIY–YIG endonuclease members. (*A*) Structure-based signature sequence alignment of AtGRXS16-NTD with other GIY–YIG endonucleases. Red dots mark the previously defined signature motifs and catalytically important residues. The green dot marks the Cys^{123} residue in AtGRXS16-NTD. (*B*) The corresponding residues in AtGRXS16-NTD are shown as sticks. (*C*) Alignment of catalytically important residues in R.Eco29KI (green) with their corresponding residues in AtGRXS16-NTD (cyan).

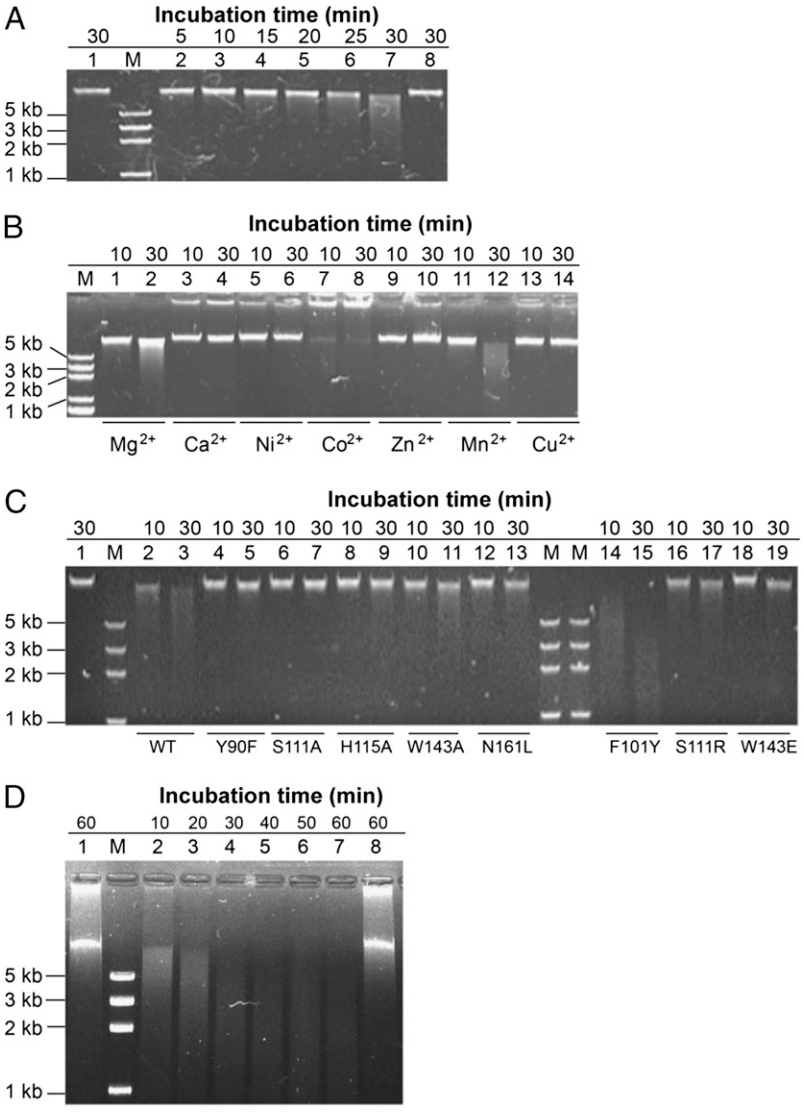

Fig. 3. In vitro dsDNA digestion assay. (*A*) dsDNA endonuclease activity. The reaction was carried out by incubating 2 μM AtGRXS16-NTD with 7.5 ng/μL λDNA in a final volume of 20 μL at 37 °C and then stopped by adding EDTA. Lanes 2–7 show the reaction products after incubation for 5, 10, 15, 20, 25, and 30 min, respectively. Lanes 1 and 8 show the products without magnesium acetate and with 50 mM EDTA in the reaction buffer, respectively. Lane M shows the marker. (*B*) Effects of divalent cations on AtGRXS16-NTD endonuclease activity. The reaction was performed in the same buffer for 10 min and 30 min with 20 mM $MgCl_2$ (lanes 1 and 2), 20 mM $CaCl_2$ (lanes 3 and 4), 20 mM $NiCl_2$ (lanes 5 and 6), 20 mM $CoCl_2$ (lanes 7 and 8), 20 mM $ZnCl_2$ (lanes 9 and 10), 20 mM $MnCl_2$ (lanes 11 and 12), and 20 mM $CuCl_2$ (lanes 13 and 14). (*C*) Effects of mutations on AtGRXS16-NTD endonuclease activity. The reaction products are shown in lanes 2–19; lane 1 shows the product with wild-type AtGRXS16-NTD in the reaction buffer without magnesium acetate. (*D*) In vitro digestion of spinach cpDNA. The reaction was carried out by incubating 5 μM AtGRXS16-NTD with 10 ng/μL cpDNA in the same reaction buffer as the digestion of λDNA (lanes 2–7). Lanes 1 and 8 are the reaction products without magnesium acetate (lane 1) and with 50 mM EDTA (lane 8).

a time-dependent manner, indicating its endonuclease activity is nonspecific and independent of its substrate sequence. We also screened several different divalent cations and found that the nuclease activity is enhanced in the presence of Mg^{2+} or Mn^{2+} but not Ca^{2+}, Ni^{2+}, Co^{2+}, Zn^{2+}, and Cu^{2+} (Fig. 3*B*).

The putative active site of AtGRXS16-NTD is nonclassical (Fig. 2*B*); therefore, we carried out mutagenesis experiments to investigate the role of each residue in the nuclease activity of AtGRXS16-NTD. Our results showed that cleavage activities of Tyr90Phe, Ser111Ala, and His115Phe mutants were significantly reduced, whereas Trp143Ala and Asn161Leu mutants still had some activity (Fig. 3*C*). The Phe101Ala mutant was insoluble during the expression and purification. We also generated Phe101Tyr, Ser111Arg, and Trp143Glu mutants by substituting the AtGRXS16-NTD–specific residues with conserved residues in other GIY–YIG endonucleases. The Phe101Tyr mutant had enhanced cleavage activity, indicating the importance of the tyrosine residue in the YIG motif for the nuclease activity (Fig. 3*C*). Both Ser111Arg and Trp143Glu mutants displayed unanticipated reduced endonuclease activities (Fig. 3*C*), which suggests that the catalytic mechanism of AtGRXS16-NTD may be unique from that of other GIY–YIG endonucleases. These AtGRXS16-NTD variants all exhibited very similar gel-filtration profiles as that of wild type (Fig. S4), suggesting changes in nuclease activity were not a result of conformational changes.

To further determine whether AtGRXS16-NTD has endonuclease activity in plants given that the protein targets to chloroplasts in vivo, we performed an in vitro endonuclease assay using chloroplastic genome DNA (cpDNA) as a substrate. AtGRXS16-NTD also digested cpDNA in a time-dependent manner (Fig. 3*D*), suggesting that AtGRXS16 may function as an endonuclease in chloroplasts.

AtGRXS16 NTD Blocks Its Grx Domain Activity to Suppress Yeast *grx5* Mutant Phenotypes. Previous reports suggest that CGFS-type monothiol Grxs bind an iron–sulfur cluster (20, 21) and suppress yeast *grx5* mutant phenotypes (8). AtGRXS16 purified from *Escherichia coli* cells displayed a dark-brown color, but the color faded quickly. A small portion of light-brown AtGRXS16 dimer could be detected and separated by gel filtration; however, the majority of purified proteins (>85%) were the colorless monomer (Fig. S5 *A* and *B*). The AtGRXS16 colorless monomer and brownish dimer were subjected to UV-visible spectra measurement immediately after the purification. Increases in absorbance at 320 nm, 410 nm, and 460 nm could be observed in the dimer, but not in the monomer (Fig. S5*C*), indicating that AtGRXS16 dimer can bind a Fe-S cluster.

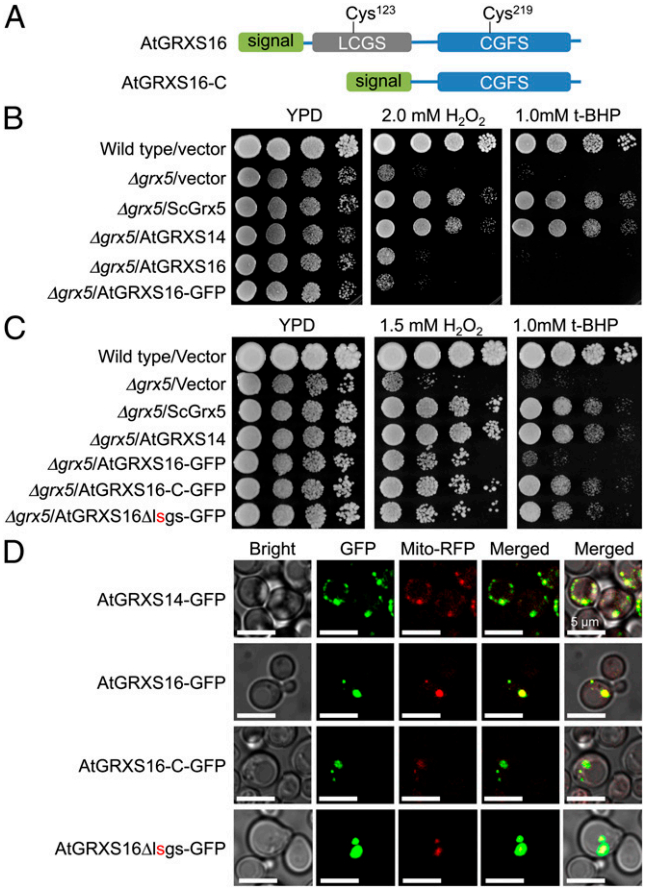

Fig. 4. Functional analysis of AtGRXS16 and its variants in yeast. (*A*) Shown are diagrams of AtGRXS16 and its mutant constructs. AtGRXS16-C was generated through the N-terminal truncation. One point-mutation construct, AtGRXS16Δlsgs, was created by changing Cys^{123} to serine residue. (*B*) AtGRXS16 is unable to suppress the sensitivity of *grx5* cells to oxidants. Wild-type and *grx5* cells expressing vector and various plasmids as indicated were assayed in YPD medium and the same medium supplemented with 2.0 mM H_2O_2 and 1.0 mM t-BHP, respectively. Photos were taken after 3 d of growth at 30 °C. Shown is one representative experiment from four independent experiments conducted. (*C*) AtGRXS16 mutants are able to suppress the sensitivity of *grx5* cells to oxidants. Wild-type and *grx5* cells expressing vector and various plasmids as indicated were assayed in the same condition as in *B*. (*D*) Subcellular localization of AtGRXS14-GFP, AtGRXS16-GFP, AtGRXS16-C-GFP, and AtGRXS16Δlsgs-GFP in yeast cells. (Scale bars: 5 μm.)

To determine whether AtGRXS16 could complement yeast ScGrx5 function and suppress the sensitivity of *grx5* cells to oxidants, such as hydrogen peroxide (H_2O_2) and *tert*-butyl hydroperoxide (tBHP), we expressed vector control, ScGrx5, AtGRXS14, and AtGRXS16 in *grx5* cells. All yeast strains grew normally in yeast peptone dextrose (YPD) medium (rich media) after 72-h growth (Fig. 4*B*). Although the growth of vector-expressing *grx5,* AtGRXS16-, and AtGRXS16-GFP–expressing cells were impaired in the medium containing H_2O_2 or tBHP, both ScGrx5- and AtGRXS14-expressing *grx5* cells grew in a similar manner that could suppress the sensitivity of *grx5* cells to oxidants (Fig. 4*B*). The inability of cells expressing AtGRXS16-GFP to suppress these phenotypes was not based on mislocalization, as the fusion protein was found predominately in mitochondria (Fig. 4*D* and Fig. S6).

AtGRXS16 consists of a single Grx domain and a NTD (Fig. S2). We speculate that the Grx domain of AtGRXS16 would function in the suppression of *grx5* cell sensitivity to oxidants. A truncated AtGRXS16 Grx domain was expressed in *grx5* cells and compared with AtGRXS16-expressing cells (Fig. 4*A*). As shown in Fig. 4*C*, AtGRXS16-C-GFP was able to rescue the growth of *grx5* cells in oxidant-containing medium, suggesting that the single Grx domain of AtGRXS16 is functional as it targeted to mitochondria in yeast (Fig. 4*D* and Fig. S6). This finding also suggests that the NTD of AtGRXS16 blocks the activity of AtGRXS16 in *grx5* cells. In the NTD of AtGRXS16, the Cys^{123} residue is conserved across species (Fig. S2). To determine whether this Cys^{123} residue is involved in inhibiting AtGRXS16 activity in *grx5* cells, a Cys single mutant, AtGRXS16Δlsgs-GFP, was generated by substituting Cys^{123} with Ser. Cells expressing this mutant suppressed the sensitivity of *grx5* cells to oxidative stress in a manner indistinguishable from cells expressing the AtGRXS16-C-GFP (Fig. 4*C*) with both proteins targeted to the mitochondria (Fig. 4*D* and Fig. S6).

Yeast Grx5 deletion mutants are defective in lysine synthesis due to disruption of the maturation of a mitochondrial Fe–S cluster-containing enzyme, homoaconitase (22). As a result, *grx5* cells fail to grow on lysine deficient medium, whereas wild-type cells grew well on the same medium (Fig. S7) (22). Cells expressing AtGRXS16-C-GFP displayed slightly more robust growth compared with *grx5* cells (Fig. S7), whereas cells expressing AtGRXS16Δlsgs-GFP was able to rescue the lysine auxotrophy of *grx5* cells (Fig. S7). This result indicates that the NTD of AtGRXS16 is required for restoration of Grx5 functions in Fe–S cluster biogenesis.

AtGRXS16 Forms an Intramolecular Disulfide Bond to Regulate Its Dual Functions. The Cys123Ser mutation enhances AtGRXS16 activity in *grx5* cells (Fig. 4*C*). We also know that Cys^{219} in the "CGFS motif" is critical for the activity of Grx domains (7). Therefore, we propose that Cys^{123} in the NTD may form an intramolecular disulfide bond with Cys^{219} in the CTD to inhibit the activity of this Grx domain. This model is supported by our mass spectrometric data showing that more than 70% of monomers are oxidized to form a disulfide linkage between SVPELCGSVK and SAPQCGFSQR peptides (Fig. 5*A* and Table S2). In contrast, we found that in the AtGRXS16 dimer, 65% of the Cys residues in the NTD (SVPELCGSVK) and 66% of the Cys residues in the CTD (SAPQCGFSQR), as readouts as free thiols in these assays, did not form an intramolecular disulfide bond (Table S2), which is consistent with the fact that the Cys residue in the "CGFS" motif is essential for Fe–S cluster binding (Fig. S5*C*) (20, 21, 23). These results also suggest that AtGRXS16-NTD could bind to the Grx domain bridged by an intramolecular disulfide bond and inhibit the Grx activity in vivo. This model is supported by the ability of AtGRXS16Δlsgs-GFP to suppress the sensitivity of *grx5* cells to oxidative stress (Fig. 4*C*), whereas when both domains of AtGRXS16 were present, the activity was blocked (Fig. 5*B*). To investigate if the intramolecular disulfide bond affects AtGRXS16 endonuclease activity, the endonuclease activity of AtGRXS16 monomer was examined and found at a reduced rate compared with AtGRXS16-NTD (Fig. 5*C*). Then, an AtGRXS16 mutant was generated by substituting both Cys^{123} and Cys^{219} with serine residues ($AtGRXS16_{\Delta Cys}$). It cleaved λDNA more efficiently than an AtGRXS16 monomer and its activity was comparable with that of AtGRXS16-NTD (Fig. 5*C*). Moreover, as expected, in AtGRXS16 dimers with most of their cysteine residues that did not form intramolecular disulfide bonds, their NTDs were active and could cleave λDNA more efficiently than the AtGRXS16 monomer (Fig. 6*A*). To further determine whether a reducing condition could affect AtGRXS16 endonuclease activity, the endonuclease activity of the AtGRXS16 monomer was examined in the presence of a reducing reagent, DTT. As shown in Fig. 6*B*, the ability of the AtGRXS16 monomer to cleave λDNA was dependent on the dosage of the reducing agent. Taken together, these results demonstrate that the formation of an intracellular disulfide bond may negatively regulate both the N-terminal endonuclease and the C-terminal Grx activities.

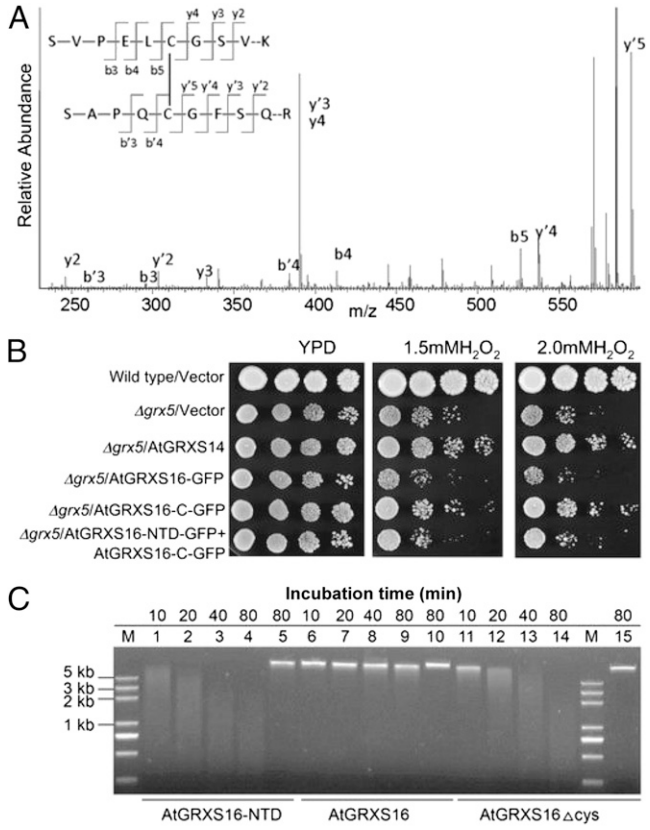

Fig. 5. Cys^{123} and Cys^{219} form an intramolecular disulfide bond that negatively regulates AtGRXS16-NTD nuclease and Grx domain activities. (*A*) The MS/MS spectrum of a triply charged precursor ion MH_3^{3+} at *m/z* 699.3353 matching to the mass of the disulfide bond-linked peptides SVPLCGSVK and SAPQCGFSQR. The major fragment ions match to masses of expected y and b ions of the linked peptide. (*B*) Wild-type and *grx5* cells expressing vector and various plasmids as indicated were assayed in the same condition as in Fig. 4. (*C*) Comparison of the endonuclease activity of AtGRXS16-NTD, AtGRXS16, and $AtGRXS16_{\Delta Cys}$. λDNA (7.5 ng/μL) was digested with the same condition as in Fig. 3. Lanes 1–5 are the reaction products with AtGRXS16-NTD for 10, 20, 40, 80, and 80 min with EDTA. Lanes 6–10 are the products for AtGRXS16 monomers. Lanes 11–15 are the products for $AtGRXS16_{\Delta Cys}$.

Discussion

Our results reveal that chloroplastic monothiol Grx, AtGRXS16, comprises two distinct functional domains, in which an N-terminal GIY–YIG motif acts as an endonuclease and a C-terminal Grx module acts as a functional monothiol Grx (Figs. 1–4 and Figs. S1, S5, and S7). We further demonstrate that the two functional domains are negatively regulated through the formation of an intramolecular disulfide bond (Figs. 5 and 6). These findings suggest a unique inhibitory mechanism underlying GRX regulation.

AtGRXS16 targets to the chloroplast, which is consistent with previous findings (Fig. S1) (24). AtGRXS16 was unable to suppress yeast mutant cells defective in mitochondrial function (Fig. 4 *B* and *D* and Fig. S5). This result was unexpected given the functional interchangeability among CGFS type Grxs (8, 17, 18). Interestingly, the poplar chloroplastic PtGRXS16 appears to target to yeast mitochondria and is functional in yeast suppression assays (25). One explanation is that the PtGRXS16 variant used in the yeast assays was a truncated form that consists of 212 amino acid (aa) residues from 85 aa to 296 aa and lacks the signal peptide and part of the N-terminal domain (Fig. S2) (25). Our study indicates that the NTD can inhibit the activity of AtGRXS16 and the truncated form (the CTD) was functional in the yeast assay (Fig. 4). Thus, we posit that PtGRXS16 is active in the yeast assay because the protein variant tested may lack its endogenous inhibitory domain.

The GIY–YIG endonuclease recognizes and cleaves DNA substrates at specific sites by forming either a homodimeric structure (19), or a protein complex (26). On the other hand, bipartite recognition sequences are a common feature among some GIY–YIG homing endonucleases (11, 27). It has also been proposed that I-TevI may form a dimer to perform high fidelity double strand cleavage (28). However, recent studies indicate that under stress conditions or acting as monomers, some GIY–YIG endonucleases lose their enzymatic fidelity (15, 29, 30). AtGRXS16-NTD can cleave both λDNA and chloroplast genomic DNA independent of DNA sequence (Fig. 3). The cleavage activity, which is different from other GIY–YIG endonucleases, does not exclude the possibility that AtGRXS16 GIY–YIG nuclease, acting in a complex could cleave DNA at specific sites. Furthermore, AtGRXS16-NTD may form a dimer through a Fe–S cluster bridged Grx-domain dimerization (Fig. S5). In the characterized Fe–S cluster bridged Grx dimers (PDB 2E7P, 2HT9, 2WCI, 2WUL, 3RHC), although the relative orientation of the two Grx modules are quite different, the N termini are ~50 Å apart on the same side of the dimer. This distance is close enough to allow AtGRXS16-NTD to form a NTD dimer, particularly considering the long linker (~30 residues) between the NTD and Grx domains.

The N-terminal Cys^{123} residue can form an intramolecular disulfide bond with the C-terminal Cys^{219} residue, which in turn reduces both endonuclease and Grx activities including Fe–S cluster binding of AtGRXS16 in vivo under oxidative stress (Figs. 3–5 and Fig. S7). In the AtGRXS16-NTD, the Cys^{123} locates at the loop connecting α1 helix and β4 strand and its side chain points outside (Fig. 2 *A* and *B*). Based on the structure of AtGRXS14 (21), the Cys^{219} in the AtGRXS16-CTD is also located on the molecular surface. The Cys^{123}–Cys^{219} intramolecular disulfide bond in AtGRXS16 may limit the conformation change of the α1 helix in the NTD, where two catalytic residues Ser111 and His115

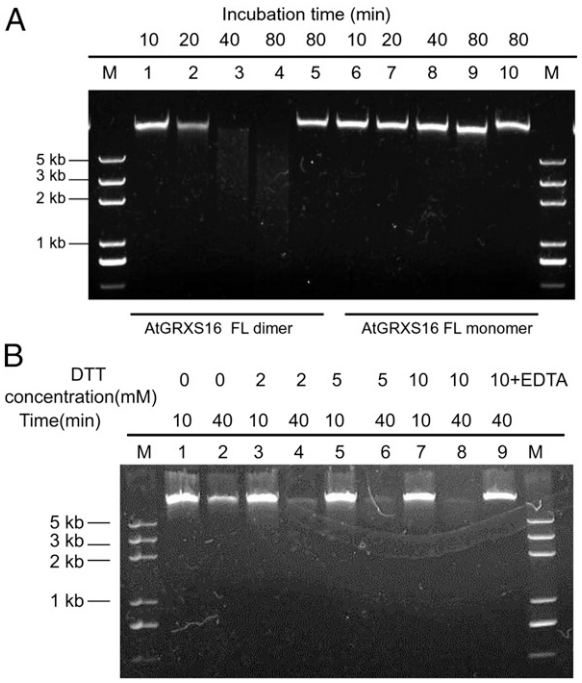

Fig. 6. Endonuclease activities of AtGRXS16 dimers and monomers in the presence of a reducing reagent. λDNA (7.5 ng/μL) was digested by AtGRXS16 dimer or monomer proteins (20 μM) (*A*) or monomer proteins (20 μM) with different concentrations of reducing reagents, DTT as indicated (*B*), in the same reaction condition as in Fig. 5*C*.

are located (Fig. 2 *A* and *B*). However, this inhibition of the oxidized monomer is reversible; under reduced environments, when the intramolecular disulfide bond is released, the hindrance is removed allowing the AtGRXS16-NTD to adjust the local active site more quickly to cleave a DNA substrate. Indeed, reduced AtGRXS16 monomers are able to efficiently digest λDNA (Fig. 6*B*). Furthermore, mutation of the Cys^{123} residue allows the Cys^{219} residue of the Grx domain to be active in a Fe–S cluster biogenesis in vivo (Fig. S7). Therefore, our data support a working hypothesis that AtGRXS16, like human Grx2 in the mitochondria, is regulated by reversible oxidation of active site cysteine residues and Fe–S cluster coordination (Fig. S8) (23, 31, 32).

Although the physiological function of AtGRXS16 is not yet clear, AtGRXS16-NTD has nuclease enzymatic activities in cleaving cpDNA (Figs. 1–3), suggesting that the N-terminal region of AtGRXS16 may be functional in the chloroplast. Given that cpDNA is under photooxidative stress during photosynthesis (4) and GIY–YIG motif containing endonucleases have been shown to play a critical role in DNA damage repair (12, 14), we speculate that AtGRXS16 may be acting as a GIY–YIG endonuclease to help mediate DNA repair in chloroplasts. It has been proposed that monothiol Grx dimers serve as a carrier to deliver the intact Fe–S cluster to the apoproteins (20) or form a [2Fe–2S] cluster–ligand complex to mediate signaling events in the cell (33). Furthermore, there is emerging evidence that Fe–S clusters become essential components of diverse nucleic acid processing machinery (34, 35) and also critical for DNA damage recognition (36). It is possible that AtGRXS16 dimers, under optimal conditions, could deliver the mature Fe–S clusters and then incorporate the clusters into nucleic acid enzymes that are required for DNA repair in the chloroplast (34). A recent report indicates that a Grx is able to regulate a GIY–YIG endonuclease, I-TevI, activity in response to oxidative stress (15), therefore, it is likely that AtGRXS16 may directly scavenge ROS and protect its target proteins from oxidation or regulate their activities through a glutathionylation and deglutathionylation mechanism in the chloroplast. Future studies will define the role of AtGRXS16 in chloroplasts.

In summary, our structural study determines that chloroplastic AtGRXS16 consists of an N-terminal GIY–YIG motif and comprises endonuclease enzyme activity. Furthermore, biochemical and functional complementation analysis demonstrates a unique regulatory mechanism underlying AtGRXS16 function in both nuclease and Grx activities. These findings provide insights into the interplay among redox regulation, DNA repair, and metabolism.

Materials and Methods

Plasmid DNA constructions, yeast strains and growth assays, localization of AtGRXS16 and its variant GFP fusions in yeast and plant cells, protein expression and purification, size exclusion chromatography and UV-visible spectra, NMR spectroscopy and structure calculations, plant materials and chloroplast genome DNA isolation, in vitro nucleic acid digestion, detection of disulfide bond formation by mass spectrometry are described in detail in *SI Materials and Methods*. They are described in the order shown above. All PCR primer sequences are listed in Table S3.

ACKNOWLEDGMENTS. We thank Drs. Toshiro Shigaki and Yule Liu for critical reading of the manuscript; Shaojie Han for assistance in chloroplast genomic DNA preparation; Likui Feng and Guangjun He for assistance with UV-Vis analyses; and Drs. Yi Wu, Lilin Du, Zhiyong Lou, Yongbin Yan, and She Chen for helpful discussion. This work is supported by the Agricultural Research Service, US Department of Agriculture under Cooperation Agreement 6250-51000-055 (to N.C.), the National Natural Science Foundation of China (31170701; to Y.F.), the Ministry of Science and Technology (2010CB912402 and 2011CB910502; to X.W.), and the Natural Science Foundation of Zhejiang Province (LY12C14001; to J.Z.L.).

1. Apel K, Hirt H (2004) Reactive oxygen species: Metabolism, oxidative stress, and signal transduction. *Annu Rev Plant Biol* 55:373–399.
2. Buchanan BB, Balmer Y (2005) Redox regulation: A broadening horizon. *Annu Rev Plant Biol* 56:187–220.
3. Finkel T, Holbrook NJ (2000) Oxidants, oxidative stress and the biology of ageing. *Nature* 408(6809):239–247.
4. Niyogi KK (1999) PHOTOPROTECTION REVISITED: Genetic and Molecular Approaches. *Annu Rev Plant Physiol Plant Mol Biol* 50:333–359.
5. Foyer CH, Noctor G (2011) Ascorbate and glutathione: The heart of the redox hub. *Plant Physiol* 155(1):2–18.
6. Lillig CH, Berndt C, Holmgren A (2008) Glutaredoxin systems. *Biochim Biophys Acta* 1780(11):1304–1317.
7. Herrero E, de la Torre-Ruiz MA (2007) Monothiol glutaredoxins: A common domain for multiple functions. *Cell Mol Life Sci* 64(12):1518–1530.
8. Molina-Navarro MM, Casas C, Piedrafita L, Bellí G, Herrero E (2006) Prokaryotic and eukaryotic monothiol glutaredoxins are able to perform the functions of Grx5 in the biogenesis of Fe/S clusters in yeast mitochondria. *FEBS Lett* 580(9):2273–2280.
9. Tripathi T, Rahlfs S, Becker K, Bhakuni V (2008) Structural and stability characteristics of a monothiol glutaredoxin: Glutaredoxin-like protein 1 from Plasmodium falciparum. *Biochim Biophys Acta* 1784(6):946–952.
10. Sundaram S, Rathinasabapathi B, Ma LQ, Rosen BP (2008) An arsenate-activated glutaredoxin from the arsenic hyperaccumulator fern Pteris vittata L. regulates intracellular arsenite. *J Biol Chem* 283(10):6095–6101.
11. Belfort M, Roberts RJ (1997) Homing endonucleases: Keeping the house in order. *Nucleic Acids Res* 25(17):3379–3388.
12. Dunin-Horkawicz S, Feder M, Bujnicki JM (2006) Phylogenomic analysis of the GIY–YIG nuclease superfamily. *BMC Genomics* 7:98.
13. Oppermann T, Hong TH, Surzycki SJ (1989) Chloroplast and nuclear genomes of Chlamydomonas reinhardtii share homology with Escherichia coli genes for DNA replication, repair and transcription. *Curr Genet* 15(1):39–46.
14. Kwon T, Huq E, Herrin DL (2010) Microhomology-mediated and nonhomologous repair of a double-strand break in the chloroplast genome of Arabidopsis. *Proc Natl Acad Sci USA* 107(31):13954–13959.
15. Robbins JB, Smith D, Belfort M (2011) Redox-responsive zinc finger fidelity switch in homing endonuclease and intron promiscuity in oxidative stress. *Curr Biol* 21(3):243–248.
16. Cheng NH, Hirschi KD (2003) Cloning and characterization of CXIP1, a novel PICOT domain-containing Arabidopsis protein that associates with CAX1. *J Biol Chem* 278(8):6503–6509.
17. Cheng NH, Liu JZ, Brock A, Nelson RS, Hirschi KD (2006) AtGRXcp, an Arabidopsis chloroplastic glutaredoxin, is critical for protection against protein oxidative damage. *J Biol Chem* 281(36):26280–26288.
18. Cheng NH (2008) AtGRX4, an Arabidopsis chloroplastic monothiol glutaredoxin, is able to suppress yeast grx5 mutant phenotypes and respond to oxidative stress. *FEBS Lett* 582(6):848–854.
19. Mak AN, Lambert AR, Stoddard BL (2010) Folding, DNA recognition, and function of GIY–YIG endonucleases: Crystal structures of R.Eco29kI. *Structure* 18(10):1321–1331.
20. Iwema T, et al. (2009) Structural basis for delivery of the intact [Fe2S2] cluster by monothiol glutaredoxin. *Biochemistry* 48(26):6041–6043.
21. Li L, Cheng N, Hirschi KD, Wang X (2010) Structure of Arabidopsis chloroplastic monothiol glutaredoxin AtGRXcp. *Acta Crystallogr D Biol Crystallogr* 66(Pt 6):725–732.
22. Rodríguez-Manzaneque MT, Tamarit J, Bellí G, Ros J, Herrero E (2002) Grx5 is a mitochondrial glutaredoxin required for the activity of iron/sulfur enzymes. *Mol Biol Cell* 13(4):1109–1121.
23. Johansson C, et al. (2011) The crystal structure of human GLRX5: Iron-sulfur cluster coordination, tetrameric assembly and monomer activity. *Biochem J* 433(2):303–311.
24. Couturier J, et al. (2011) Arabidopsis chloroplastic glutaredoxin C5 as a model to explore molecular determinants for iron-sulfur cluster binding into glutaredoxins. *J Biol Chem* 286(31):27515–27527.
25. Bandyopadhyay S, et al. (2008) Chloroplast monothiol glutaredoxins as scaffold proteins for the assembly and delivery of [2Fe-2S] clusters. *EMBO J* 27(7):1122–1133.
26. Truglio JJ, Croteau DL, Van Houten B, Kisker C (2006) Prokaryotic nucleotide excision repair: The UvrABC system. *Chem Rev* 106(2):233–252.
27. Bell-Pedersen D, Quirk SM, Bryk M, Belfort M (1991) I-TevI, the endonuclease encoded by the mobile td intron, recognizes binding and cleavage domains on its DNA target. *Proc Natl Acad Sci USA* 88(17):7719–7723.
28. Van Roey P, Meehan L, Kowalski JC, Belfort M, Derbyshire V (2002) Catalytic domain structure and hypothesis for function of GIY–YIG intron endonuclease I-TevI. *Nat Struct Biol* 9(11):806–811.
29. Bryk M, et al. (1993) The td intron endonuclease I-TevI makes extensive sequence-tolerant contacts across the minor groove of its DNA target. *EMBO J* 12(10):4040–4041.
30. Bryk M, Belisle M, Mueller JE, Belfort M (1995) Selection of a remote cleavage site by I-tevI, the td intron-encoded endonuclease. *J Mol Biol* 247(2):197–210.
31. Berndt C, et al. (2007) How does iron-sulfur cluster coordination regulate the activity of human glutaredoxin 2? *Antioxid Redox Signal* 9(1):151–157.
32. Johansson C, Kavanagh KL, Gileadi O, Oppermann U (2007) Reversible sequestration of active site cysteines in a 2Fe-2S-bridged dimer provides a mechanism for glutaredoxin 2 regulation in human mitochondria. *J Biol Chem* 282(5):3077–3082.
33. Li H, et al. (2011) Histidine 103 in Fra2 is an iron-sulfur cluster ligand in the [2Fe-2S] Fra2-Grx3 complex and is required for in vivo iron signaling in yeast. *J Biol Chem* 286(1):867–876.
34. White MF, Dillingham MS (2012) Iron-sulphur clusters in nucleic acid processing enzymes. *Curr Opin Struct Biol* 22(1):94–100.
35. Wu Y, Brosh RM, Jr. (2012) DNA helicase and helicase-nuclease enzymes with a conserved iron-sulfur cluster. *Nucleic Acids Res* 40(10):4247–4260.
36. Kuper J, Kisker C (2012) Damage recognition in nucleotide excision DNA repair. *Curr Opin Struct Biol* 22(1):88–93.

Supporting Information

Liu et al. 10.1073/pnas.1306899110

SI Materials and Methods

Plasmid DNA Constructs, Yeast Strains, and Growth Assays. The full-length cDNA of *Arabidopsis thaliana* glutaredoxin S16 (AtGRXS16), originally named CXIP2 (1), was amplified by PCR using a gene-specific primer (Table S3). To create a C-terminal truncated form (AtGRXS16-C), the chloroplast-targeting signal peptide (62 aa at its N terminus), that was predicted by the Chloro P (version 1.1) program, was amplified with AtGRXS16 forward and AtGRXS16-signal-reverse primers (Table S3), and the AtGRXS16 glutaredoxin (Grx) domain was amplified with AtGRXS16-C forward and AtGRXS16-gfp-reverse primers (Table S3). The XbaI/HindIII fragment of the signal peptide and the HindIII/BamHI fragment of the AtGRXS16 Grx domain were cloned into pBluescript at XbaI/BamHI sites through a three-way ligation to make the AtGRXS16-C construct. To generate an N-terminal domain (NTD), the AtGRXS16-NTD (1–163 amino acids including the first 62-aa signal peptide) was amplified with AtGRXS16-forward and AtGRXS16-NTD-reverse primers. Site-directed mutagenesis was performed as described (2). AtGRXS16-NTD-Cys-forward and AtGRXS16-NTD-Cys-reverse primers were used for creating the C123S mutation in the NTD. AtGRXS16-C-Cys-forward and AtGRXS16-C-Cys-reverse primers were used for creating the C219S mutation in the Grx-domain. PCR fragments were cloned into pT-easy vector (Promega). ScGrx3-flag and AtGRXS14-flag genes were amplified by PCR with the gene-specific primers (Table S3) and cloned into the pGEM-Teasy vector. The fidelity of all clones was confirmed by sequencing. To express in yeast cells, the full-length cDNA of *AtGRXS16* and its mutants was subcloned into yeast Ura3-marked expression vector with a glyceraldehyde-3-phosphate dehydrogenase gene (GPD) promoter, piUGpd (3). *Saccharomyces cerevisiae* wild-type strain CML235 (*MAT*a *ura3–52 leu2_1 his3_200*), *grx5* (*MAT*a *ura3–52 leu2_1 his3_200 grx5*::*kanMX4*) were provided by Enrique Herrero (Universitat de Lleida, Lleida, Spain) and used in all yeast experiments. Yeast cells were transformed by using the LiOAc method (4). All yeast strains were assayed on yeast peptone dextrose (YPD) medium (rich medium) with or without various concentrations of H_2O_2 and tert-butyl hydroperoxide (tBHP) (5).

Localization of AtGRXS16 and Its Variant GFP Fusions in Yeast and Plant Cells. To generate AtGRXS16 and its mutant GFP fusion, full-length AtGRXS16 or its mutant was cut with XbaI/BamHI sites, and the GFP gene was cut with BamHI/SstI sites. Two fragments were cloned into a piUGpd vector or pRTL2 vector that was cut with XbaI/SstI sites through a three-way ligation as described (4). In plant cells, the subcellular localization of AtGRXS16-GFP was imaged in comparison with AtGRXS14-GFP and chloroplast fluorescence as described (5). In yeast, AtGRXS16-GFP or its mutant fusion was imaged in comparison with AtGRXS14-GFP and the mitochondrial marker, COX6a-DsRed fusion as described (5).

Isolation of Mitochondrial Fractions and Western Blot Analysis. Yeast *grx5* cells expressing ScGrx5-Flag, AtGRXS14-Flag, AtGRXS16-GFP, AtGRXS16-C-GFP, and AtGRXS16-Δlsgs-GFP were grown exponentially in YPG medium at 30 °C. Yeast mitochondria were purified and fractionated following published protocols (6, 7). Forty micrograms of protein lysates were loaded on 12% SDS/PAGE gel and then transferred onto PVDF membrane. Western blot was conducted to detect tagged GRXs in mitochondrial fraction. Monoclonal anti-Flag antibody (M2, Sigma-Aldrich) was used at 1:1,000 dilution to detect ScGrx5-Flag and AtGRXS14-Flag. Polyclonal anti-GFP antibody (Cell Signaling) was used at 1:1,000 dilutions to detect the GFP fusion of AtGRXS16 and its variants. Anti-Lipoic Acid antibody (ab58724, Abcam) was used at 1:2,000 dilutions to detect the matrix markers pyruvate dehydrogenase (PDH) and α-ketoglutarate dehydrogenase (α-KGDH).

Protein Expression and Purification. The coding sequences of mature AtGRXS16 (residues 63–293), the NTD (residues 63–173) and their mutants were cloned into pET-22b vector (Novagen) with C-terminal His tag. *Escherichia coli* BL21 (DE3) cells harboring the expression construct were grown at 310 K in LB medium containing 100 mg/L ampicillin. At OD_{600} of 0.6–0.8, expression of target proteins was induced by addition of isopropyl β-D-1-thiogalactopyranoside (IPTG) to a final concentration of 0.6 mM. After further incubation at 289 K overnight, the cells were pelleted and resuspended in lysis buffer (10 mM Hepes, pH 7.2/150 mM NaCl/20 mM imidazole) and lysed by sonication. The complete lysates were centrifuged at 20,000 × *g* at 277 K for 40 min, and the supernatant containing the His-tagged protein was transferred onto a Ni-NTA column, which was then washed extensively with lysis buffer. The bound His-tagged proteins were eluted with elution buffer (10 mM Hepes, pH 7.2/150 mM NaCl/250 mM imidazole). The eluted protein was further purified on a Superdex-200 gel-filtration column and concentrated to a concentration of 2–3 mg/mL in 10 mM Hepes (pH 7.2)/150 mM NaCl.

Size Exclusion Chromatography and UV-Visible Spectra. Gel-filtration analysis of purified AtGRXS16 was carried out at 277 K on a prepacked Superdex 200 10/300 column on an ÄKTA-FPLC, equilibrated and run with the above mentioned buffer. Sample with a volume of 1 mL was injected into the column. Elution profiles were recorded at 280 nm under a constant flow rate of 0.5 mL/min. The separation of the monomeric and dimeric AtGRXS16 by gel-filtration chromatography was performed on the same column. UV-visible spectra were monitored between 200 and 800 nm at the Ultraspec 4300 pro UV/visible spectrophotomer (Beckman).

NMR Spectroscopy and Structure Calculations. All NMR experiments were performed at 298 K on a Bruker DMX 600 MHz spectrometer equipped with a z-gradient triple-resonance cryoprobe. NMR samples of AtGRXS16 NTD contained 0.5–1.0 mM protein in 50 mM sodium phosphate buffer (pH 7.0), 10 mM DTT, 0.02% (wt/vol) sodium 2,2-dimethylsilapentane-5-sulfonate (DSS), and 10% (vol/vol) D_2O. Two-dimensional ^{1}H-^{15}N and ^{1}H-^{13}C heteronuclear single quantum coherence (HSQC), 3D HNCA, CBCA(CO)NH, HNCACB, HNCO, HBHA(CO)NH, HCCH-TOCSY, HCCH-COSY, CCH-TOCSY, and ^{15}N TOCSY-HSQC experiments (8) were performed for backbone and side chain assignments of AtGRXS16 NTD. Three-dimensional ^{1}H-^{15}N and ^{1}H-^{13}C NOESY-HSQC spectra with mixing times of 150 ms were collected to generate distance restraints. All data were processed with Felix (Accelrys) and analyzed with NMRViewJ (9). Proton chemical shifts were referenced to the internal DSS, and ^{15}N and ^{13}C chemical shifts were referenced indirectly (10). Initial structures of AtGRXS16-NTD were generated using the CANDID module of the CYANA software (11), and the NOE assignments given by CANDID were checked manually. The structures were refined in explicit water using CNS (12) and RECOORDScript (13). Interproton distance restraints were obtained by NMRViewJ

from the NOE peaks of 3D ^{1}H-^{15}N and ^{1}H-^{13}C NOESY-HSQC spectra. According to the peak volumes, all assigned NOEs were grouped into four classes of distance restraints: 1.8–2.8 Å, 1.8–3.7 Å, 1.8–5.5 Å, and 1.8–6.5 Å. Backbone dihedral angle restraints obtained using TALOS+ (14), as well as hydrogen-bond restraints according to the regular secondary structure patterns, were also incorporated into the structural calculation. One hundred structures were calculated by CNS, and the 50 lowest-energy structures were selected to be refined in explicit water. The 20 lowest-energy structures in the refinement were selected to represent the final ensemble of structures for AtGRXS16-NTD. The quality of the determined structures was analyzed using MOLMOL (15) and PROCHECK-NMR (16).

In Vitro Nucleic Acid Digestion. λDNA used as a dsDNA substrate was purchased from Takara, and spinach chloroplast DNA (cpDNA) was extracted and purified following published protocol (17). In vitro λ-DNA digestion was carried out by incubating 0.02 mg/mL (2 μM) AtGRXS16-NTD with λ-DNA (7.5 ng/μL) at 310 K in a final volume of 20 μL. The reaction buffer contained 50 mM potassium acetate, 20 mM Tris-acetate (pH 7.9), and 10 mM magnesium acetate. The nuclease activities of AtGRXS16-NTD mutants were tested by using the same reaction system. The effects of divalent cations on AtGRXS16-NTD nuclease activity were tested by using the same reaction buffer and incubating λ-DNA with protein in the presence of different metal salts. In vitro cpDNA digestion was carried out by incubating 0.05 mg/mL (5 μM) ATGRXS16-NTD with cpDNA substrate (10 ng/μL) at 310 K in a final volume of 20 μL. To compare the nuclease activity of AtGRXS16 with that of $AtGRXS16_{\Delta Cys}$ and AtGRXS16-NTD, a higher concentration (20 μM) of protein was used in the reaction system. All reactions were stopped by the addition of EDTA to a final concentration of 50 mM, and the reaction products were loaded into 1% agarose gels stained with ethidium bromide.

Detection of Disulfide Bond Formation by Mass Spectrometry. To identify disulfide-linked peptides, samples were separated on 1D SDS/PAGE under the nonreducing condition. The gel bands corresponding to the targeted protein were excised, followed by in-gel digestion with sequencing grade modified trypsin (Promega) in 50 mM ammonium bicarbonate at 37 °C overnight. Peptides were extracted twice with 1% trifluoroacetic acid in 50% acetonitrile aqueous solution for 30 min. The extract was then centrifuged in a speedvac to reduce the volume. To determine the ratio of a cysteine residue in disulfide bond to that in the reduced (free thiol) form, the free cysteine in samples was first modified by ^{13}C-idoacetic acid, followed by the separation of proteins by 1D SDS/PAGE. Gel bands containing the targeted protein were excised from the gel, modified again by 55 mM ^{13}C-idoacetic acid, followed by in-gel reduction with 10 mM DTT. The newly generated free cysteines were alkylated with 55 mM iodoacetamide. For LC-MS/MS analysis, the digestion product was separated by a 65-min gradient elution at a flow rate of 0.250 μL/min by using the EASY-nLCII integrated nano-HPLC system (Proxeon), which was directly interfaced with the Thermo LTQ-Orbitrap mass spectrometer. The analytical column was a home-made fused silica capillary column (75-μm i.d., 150 mm length; Upchurch) packed with C-18 resin (300 A, 5 μm, Varian). Mobile phase A consisted of 0.1% formic acid, and mobile phase B consisted of 100% acetonitrile and 0.1% formic acid. The LTQ-Orbitrap mass spectrometer was operated in the data-dependent acquisition mode using the Xcalibur 2.0.7 software, and there was a single full-scan mass spectrum in the Orbitrap (400–1,800 *m/z*, 30,000 resolution) followed by 20 data-dependent MS/MS scans in the ion trap at 35% normalized collision energy. The MS/MS spectra from each LC-MS/MS run were searched against the selected database using an in-house Mascot or Proteome Discover searching algorithm. For AtGRXS16 dimers, the quantity of the readout-free cysteines included both reduced thiols and Fe–S binding thiols because the Fe–S clusters were destroyed through 1D SDS/PAGE and the coordinating cysteines become free.

1. Cheng NH, Hirschi KD (2003) Cloning and characterization of CXIP1, a novel PICOT domain-containing Arabidopsis protein that associates with CAX1. *J Biol Chem* 278(8): 6503–6509.
2. Shigaki T, Cheng NH, Pittman JK, Hirschi K (2001) Structural determinants of Ca^{2+} transport in the Arabidopsis H^{+}/Ca^{2+} antiporter CAX1. *J Biol Chem* 276(46):43152–43159.
3. Nathan DF, Vos MH, Lindquist S (1999) Identification of SSF1, CNS1, and HCH1 as multicopy suppressors of a Saccharomyces cerevisiae Hsp90 loss-of-function mutation. *Proc Natl Acad Sci USA* 96(4):1409–1414.
4. Cheng NH, Liu JZ, Brock A, Nelson RS, Hirschi KD (2006) AtGRXcp, an Arabidopsis chloroplastic glutaredoxin, is critical for protection against protein oxidative damage. *J Biol Chem* 281(36):26280–26288.
5. Cheng NH (2008) AtGRX4, an Arabidopsis chloroplastic monothiol glutaredoxin, is able to suppress yeast grx5 mutant phenotypes and respond to oxidative stress. *FEBS Lett* 582(6):848–854.
6. Diekert KIPM, de Kroon A, Kispal G, Lill R (2001) Isolation and subfractionation of mitochondria from the yeast Saccharomyces cerevisiae. *Methods Cell Biol* 65:37–51.
7. Molina-Navarro MM, Casas C, Piedrafita L, Bellí G, Herrero E (2006) Prokaryotic and eukaryotic monothiol glutaredoxins are able to perform the functions of Grx5 in the biogenesis of Fe/S clusters in yeast mitochondria. *FEBS Lett* 580(9):2273–2280.
8. Ferentz AE, Wagner G (2000) NMR spectroscopy: A multifaceted approach to macromolecular structure. *Q Rev Biophys* 33(1):29–65.
9. Johnson BA (2004) Using NMRView to visualize and analyze the NMR spectra of macromolecules. *Methods Mol Biol* 278:313–352.
10. Markley JL, et al. (1998) Recommendations for the presentation of NMR structures of proteins and nucleic acids—IUPAC-IUBMB-IUPAB Inter-Union Task Group on the standardization of data bases of protein and nucleic acid structures determined by NMR spectroscopy. *Eur J Biochem* 256(1):1–15.
11. Güntert P, Mumenthaler C, Wüthrich K (1997) Torsion angle dynamics for NMR structure calculation with the new program DYANA. *J Mol Biol* 273(1):283–298.
12. Brünger AT, et al. (1998) Crystallography & NMR system: A new software suite for macromolecular structure determination. *Acta Crystallogr D Biol Crystallogr* 54(Pt 5): 905–921.
13. Nederveen AJ, et al. (2005) RECOORD: A recalculated coordinate database of 500+ proteins from the PDB using restraints from the BioMagResBank. *Proteins* 59(4): 662–672.
14. Shen Y, Delaglio F, Cornilescu G, Bax A (2009) TALOS+: A hybrid method for predicting protein backbone torsion angles from NMR chemical shifts. *J Biomol NMR* 44(4):213–223.
15. Koradi R, Billeter M, Wüthrich K (1996) MOLMOL: A program for display and analysis of macromolecular structures. *J Mol Graph* 14(1):51–55, 29–32.
16. Laskowski RA, Rullmannn JA, MacArthur MW, Kaptein R, Thornton JM (1996) AQUA and PROCHECK-NMR: Programs for checking the quality of protein structures solved by NMR. *J Biomol NMR* 8(4):477–486.
17. van Ee JH, Veld WAMIT, Planta RJ (1980) Isolation and Characterization of Chloroplast DNA from the Duckweed Spirodela oligorrhiza. *Plant Physiol* 66(4): 572–575.

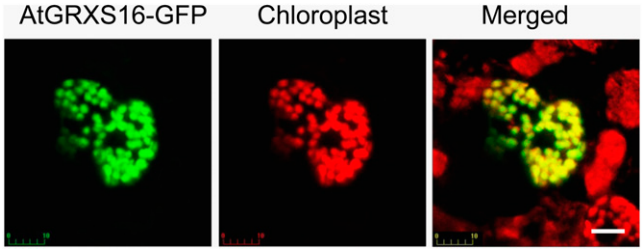

Fig. S1. AtGRXS16 protein localization. AtGRXS16-GFP was transient expressed in tobacco mesophyll cells and the subcellular localization of AtGRXS16-GFP and chloroplast autofluoresence were imaged by confocal microscopy. (Scale bars: 10 μm.)

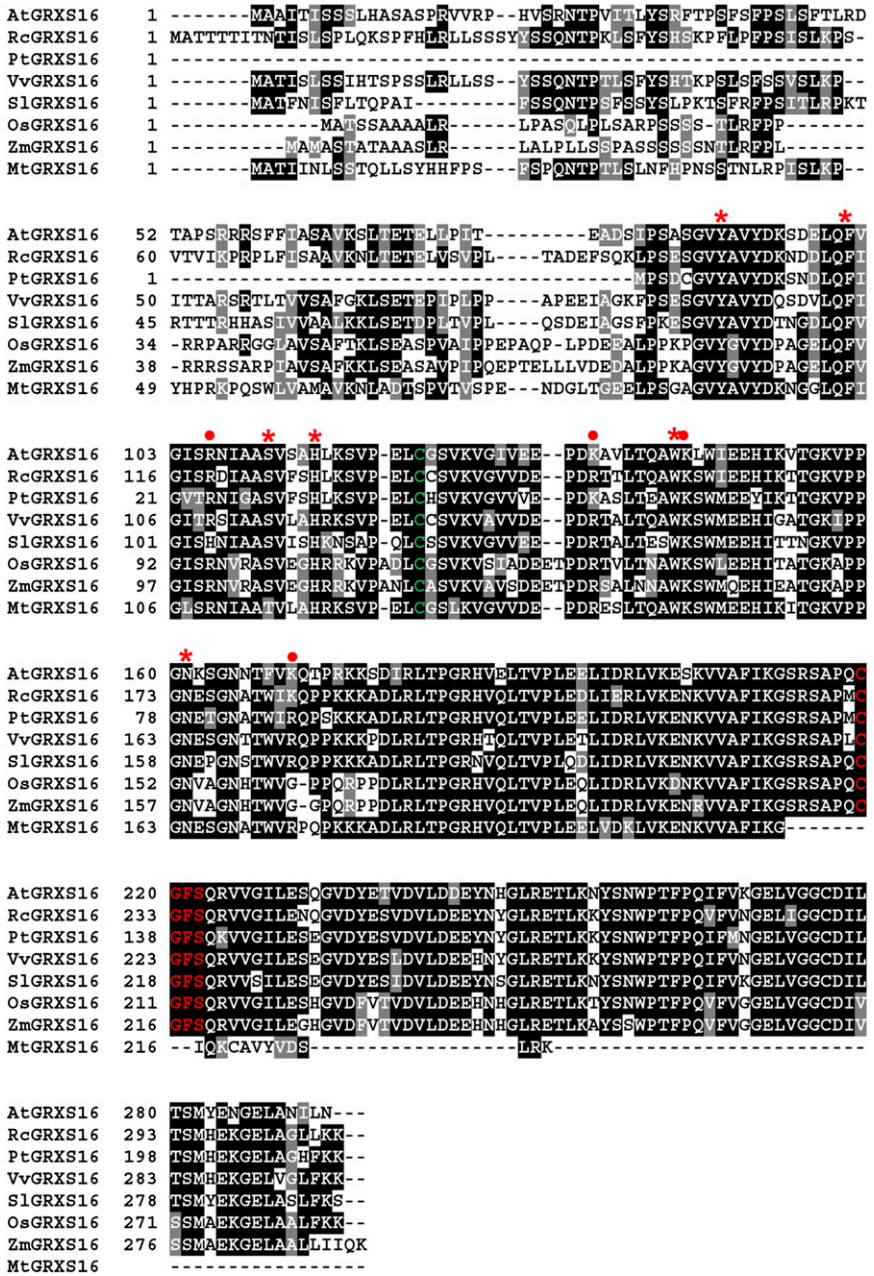

Fig. S2. Sequence analyses of AtGRXS16 homologs. Alignment of monothiol GRXS16 sequences was performed with ClustalW software (www.ebi.ac.uk/Tools/msa/clustalw2/). The conserved putative motif "CGFS" was highlighted as red, and the cysteine residue was highlighted as green. Red asterisks indicate the conserved residues that are critical for AtGRXS16 nuclease activity. Red dots indicate the positive charged residues that may involved in the binding of substrate DNA. AtGRXS16 (At2g38270), MtGRXS16, OsGRXS16 (GeneID: 4351647), PtGRXS16 (GeneID: 7466088), RcGRXS16 (GeneID: 8286336), SlGRXS16 (SlGRX1), VvGRXS16 (GeneID: 100245544), and ZmGRXS16. At, *Arabidopsis thaliana*; Mt, *Medicago truncatula*; Os, *Oryza sativa*; Pt, *Populus trichocarpa*; Sl, *Solanum lycopersicum*; Rc, *Ricinus communis*; Vv, *Vitis vinifera*; and Zm, *Zea mays*.

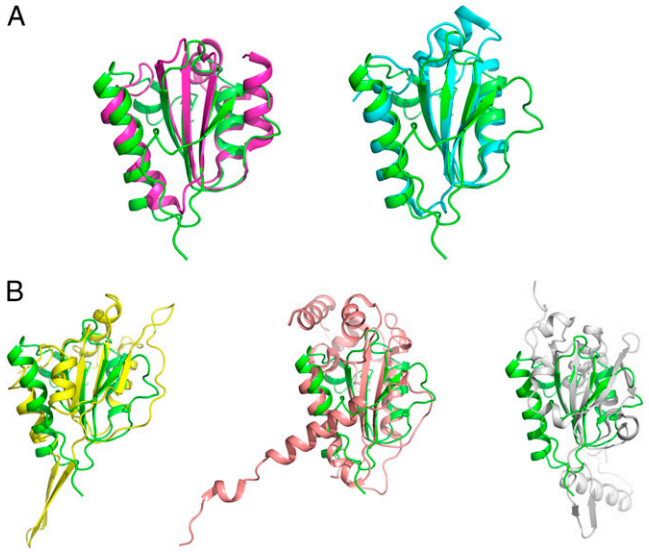

Fig. S3. Structural comparison of AtGRXS16-NTD with other GIY–YIG endonucleases. (*A*) Structural alignments of AtGRXS16-NTD (green) with UvrC (magenta, PDB ID 1YD0) and I-TevI (cyan, PDB ID 1LN0). (*B*) Structural alignments of AtGRXS16-NTD (green) with T4 EndoII (yellow, PDB ID 2WSH), R.Eco29KI (brown, PDB ID 3MX1), and Hpy188I (gray, PDB ID 3OQG).

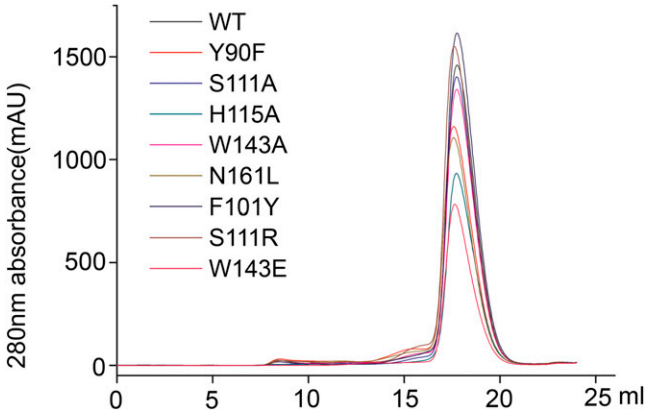

Fig. S4. The gel-filtration purification profiles of wild-type AtGRXS16-NTD and its mutants.

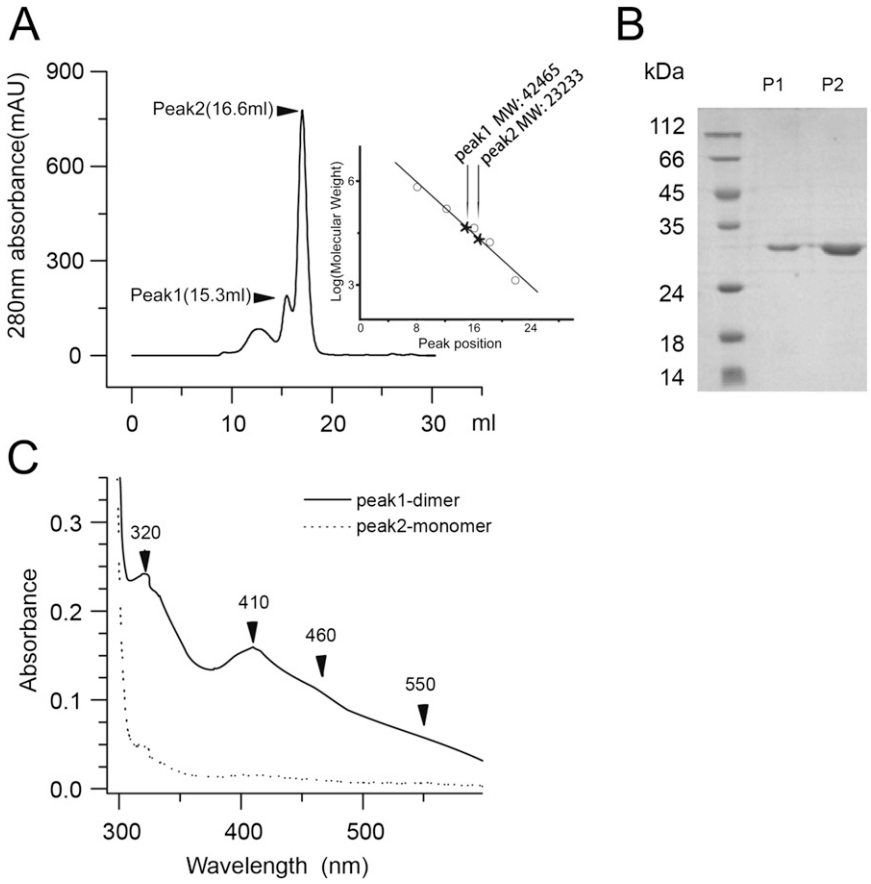

Fig. S5. Gel-filtration and UV–visible (vis) analyses of AtGRXS16. (*A*) Gel-filtration elution profile of AtGRXS16. The insert is a plot of log molecular weight against elution volume for the column. Gel filtration standards (Bio-Rad) used in the experiment were vitamin B12 (1.3 kDa), horse myoglobin (17 kDa), chicken ovalbumin (44 kDa), bovine gamma-globulin (158 kDa), and bovine thyroglobulin (670 kDa). Theoretical molecular weight of AtGRXS16 monomer is 26 kDa. Calculated molecular weights of peak 1 and peak 2 are 42,465 and 23,233 Da, respectively, indicating that these two peaks correspond with AtGRXS16 dimeric and monomeric forms, respectively. The small peak in front of the dimer and monomer peaks is a few AtGRXS16 oligomers. (*B*) SDS/PAGE gel of monomeric and dimeric peaks. (*C*) UV-vis spectra of monomeric and dimeric AtGRXS16.

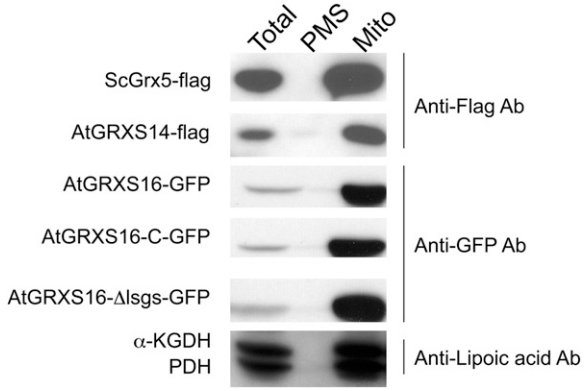

Fig. S6. AtGRXS16 and its mutants are targeting to mitochondria in yeast. Yeast cells (Δ*grx5*) expressing ScGrx5-Flag, AtGRXS14-Flag, AtGRXS16-GFP, AtGRXS16-C-GFP, and AtGRXS16-Δlsgs-GFP were grown exponentially in YPG medium at 30 °C and then fractionated, and the resulting fractions were analyzed by Western blot. Anti-Flag antibody was used to detect ScGrx5 and AtGRXS14, and anti-GFP antibody was used to detect AtGRXS16 and its mutants, and anti-lipoic acid antibody was used to detect the matrix markers pyruvate dehydrogenase (PDH) and α–ketoglutarate dehydrogenase (α-KGDH). Forty micrograms of protein were loaded in each lane for "Total" cell extracts, postmitochondrial supernatant (PMS) fractions, and the mitochondrial (Mito) fractions.

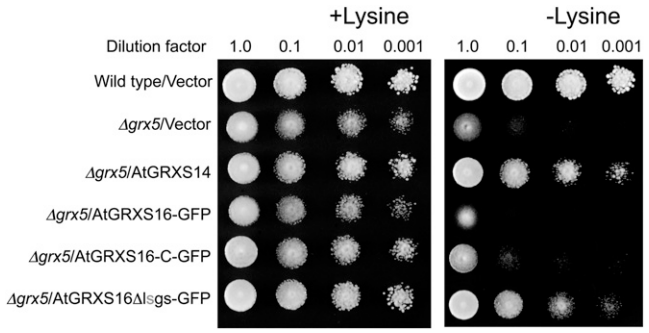

Fig. S7. Activated AtGRXS16 rescues the lysine auxotrophy of *grx5* mutant cells. Wild-type expressing vector, *grx5* cells expressing vector, AtGRXS14, AtGRXS16-GFP, AtGRXS16-C-GFP, and AtGRXS16ΔIsgs-GFP were assayed on SC medium with or without lysine. The photographs were taken after 3 d of growth at 30 °C.

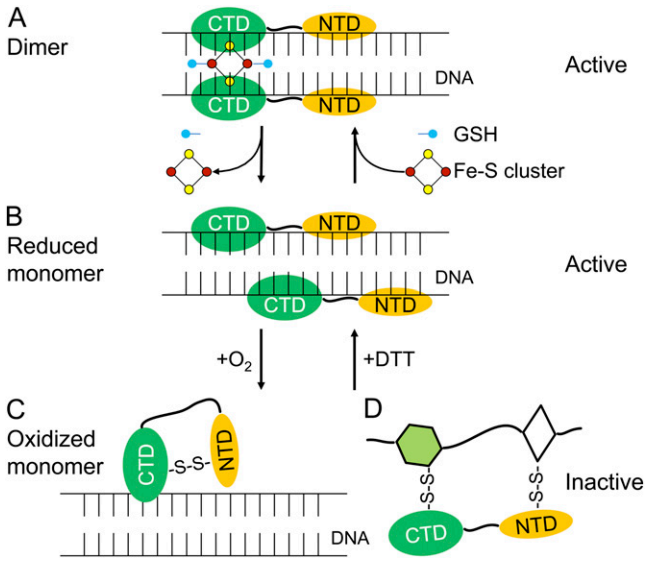

Fig. S8. A working model for AtGRXS16 in chloroplast. Our structural studies and biochemical analyses support a working hypothesis that AtGRXS16 functions in chloroplasts/plastids through a regulatory mechanism mediated by reversible oxidation of active site cysteine residues and Fe–S cluster coordination. The C-terminal Grx domain can form a Fe–S cluster complex as a dimer to deliver the mature Fe–S clusters, whereas the N-terminal domain of AtGRXS16 containing a GIY–YIG fold, which is functional in endonuclease activity, could access and bind to nucleic acid at the specific sites guided by a Grx-2Fe2S-protein complex (*A*). Reduced monomers with free active site cysteine residues are functional in both endonuclease activity and Fe–S cluster biogenesis (*B*); however, under oxidative stress, the active site cysteine residues form an intramolecular disulfide bond and then block the activities for both NTD and C-terminal domain (CTD) (*C*). AtGRXS16 can also directly scavenge reactive oxygen species (ROS) and protect its target proteins from oxidation through a glutathionylation and de-glutathionylation mechanism (*D*). In both cases, AtGRXS16 is inactive in endonuclease activity. The disulfide bond is reversible, in the presence of reducing reagents, the activity of the NTD of AtGRXS16 can be restored.

Table S1. Experimental restraints and structural statistics for the 20 lowest-energy structures of AtGRXS16 NTD

	AtGRXS16-NTD
Distance restraints	
Intraresidue	589
Sequential	515
Medium	287
Long-range	439
Ambiguous	1,095
Total	2,925
Hydrogen bond restraints	74
Dihedral angle restraints	
ϕ	85
ψ	85
Total	170
Violations	
NOE violations (>0.2 Å)	0
Largest NOE violation, Å	0.18
Torsion angle violation (>5°)	0
Largest torsion angle violation, °	3.28
PROCHECK statistics, %	
Most favored regions	82.7
Additional allowed regions	16.0
Generously allowed regions	0.6
Disallowed regions	0.7
RMSD from mean structure, Å	
Backbone heavy atoms	
All residue*	0.48 ± 0.06
Regular secondary structure†	0.39 ± 0.06
All heavy atoms	
All residue*	0.82 ± 0.07
Regular secondary structure†	0.64 ± 0.06

*Residues 66–162 in AtGRXS16-NTD.
†Residues 73–76, 88–93, 99–105, 108–117, 125–130, 136–153, and 159–162 in AtGRXS16-NTD.

Table S2. Formation of disulfide bond in the dimer and the monomer of AtGRXS16

	Cys residue in NTD*			Cys residue in CTD*		
AtGRXS16 form	Free	Total	Ratio	Free	Total	Ratio
Dimer	3.11E8	4.75E8	0.65	2.29E8	3.45E8	0.66
Monomer	2.95E8	1.32E9	0.23	4.58E8	1.51E9	0.3

*Mass spectrometric responses were used to quantify ratios of free to total cysteines in peptides from SerValProGluLeuCysGlySerValLys (SVPELCGSVK) of NTD and SerAlaProGlnCysGLyPheSerGlnArg (SAPQCGFSQR) of CTD.

Table S3. Primers used to clone AtGRXS16 gene and generate its mutant variants

Primers	Primer sequences
AtGRXS16 Forward	CCG GGG ATC CGT ATG GCT GCA ATC ACC ATT TC
AtGRXS16 Reverse	GGC GCC GCG GCT CGA GTC GAC CTA GTT CAA GAT ATT GGC
AtGRXS16-gfp-Forward	GGG CTC GAG TCT AGA ATG GCT GCA ATC ACC ATT
AtGRXS16-gfp-Reverse	GCC GAG CTC TAG GAT CCC GTT CAA GAT ATT GGC AAG
AtGRXs16-promoter-Forward	CCC AAG CTT CAT ACT GTT TTA ACT TGG ATT
AtGRXS16-promoter-Reverse	GGC TCT AGA TTT TGT CGG AGC TGA GAA AAG
AtGRXS16-signal-Reverse	GGC AAG CTT GAT AAA GAA GGA ACG ACG
AtGRXS16-NTD-Forward	GGG TCT AGA ATG GCC TCC GCC GTC AAA TCT CTA
AtGRXS16-NTD-Reverse	GGC GAG CTC TCA TAG GAT CCC TGA CTT ATT CCC CGG CGG AAC
AtGRXS16-C-Forward	GGC AAG CTT GGG AAC AAC ACA TTT GTC AAA
AtGRXS16-NTD-Cys-Forward	GAA TCC CGT CTC GAG CTT AGC CGC TCC GTT AAG GTT GGA ATA
AtGRXS16-NTD-Cys-Reverse	GAA TTC CGT CTC AAG CTC CGG CAC AGA TTT GAG
AtGRXS16-C-Cys-Forward	GAA TCC CGT CTC CCT CAA AGC GGA TTC TCA CAG AGA GTT GTT
AtGRXS16-C-Cys-Reverse	GAA TTC CGT CTC TTG AGG AGC ACT CCT TGA TCC
ScGrx5 forward	GCC GGA TCC ATG TTT CTC CCA AAA TTC AAT
ScGrx5-flag-reverse	CCG GAG CTC TCA **TCC CTT GTC GTC ATC GTC TTT GTA GTC** ACG ATC TTT GGT TTC TTC
AtGRXS14 forward	GGG CTC GAG AGA TCT GCG ATG GCT CTC CGA TCT GTC AAA
AtGRXS14-flag reverse	GGC GAG CTC TCA **TCC CTT GTC GTC ATC GTC TTT GTA GTC** AGA GCA CAT AGC TTT CTC

The underlines represent the sites of restriction enzymes and the bold letters represent the Flag tag sequences.